Inducing Regioselective Chemical Reactivity in Graphene with Alkali Metal Intercalation

Journal:	*Physical Chemistry Chemical Physics*
Manuscript ID	CP-ART-05-2018-002903.R1
Article Type:	Paper
Date Submitted by the Author:	25-Jun-2018
Complete List of Authors:	Mitchell, Izaac; The University of Newcastle, Discipline of Chemistry Irle, Stephan ; Oak Ridge National Laboratory, Computational Science and Engineering Division Page, Alister; The University of Newcastle, Discipline of Chemistry

Journal Name

ARTICLE

Inducing Regioselective Chemical Reactivity in Graphene with Alkali Metal Intercalation

Received 00th January 20xx,
Accepted 00th January 20xx

DOI: 10.1039/x0xx00000x

www.rsc.org/

Izaac Mitchell,[a] Stephan Irle,[b] Alister J. Page[a]*

First principles calculations demonstrate that alkali metal atoms, intercalated between metal substrates and adsorbed graphene monolayers, induce localised regions of increased reactivity in adsorbed graphene monolayers. The extent of this localisation is proportional to the size of the alkali atom and the strength of the graphene-substrate interaction. Thus, larger alkali atoms are more effective (e.g. K>Na>Li), as are stronger-interacting substrates (e.g. Ni>Cu). Despite the electropositivity of these alkali metal adsorbates, analysis of charge transfer phenomena between the alkali metal, the substrate and the adsorbed graphene layer indicates that charge transfer does not give rise to the observed regioselective reactivity. Instead, the increased reactivity induced in the graphene structure is attributed to the geometrical distortion of the graphene layer imposed by the intercalated adsorbed atom. We show that this strategy can be used with arbitrary adsorbates and substrate defects, provided such structures are stable, towards controlling the mesoscale patterning and chemical functionalisation of graphene structures.

Introduction

Graphene is a 2-dimensional monolayer allotrope of carbon consisting of carbon atoms arranged in a hexagonal lattice. The remarkable physicochemical properties of graphene (e.g. high specific surface area,[1] thermal conductivity,[2] mechanical strength,[3] high carrier mobilities,[4] etc.) have driven intense study toward its potential applications. These include chemical technologies such as ion batteries,[5] hydrogen storage,[6] gas sensing,[7] single molecule detection,[8] ultra-fast DNA sequencing,[9] and green chemistry applications.[10]

Despite these advances, controlling the properties and reactivity of graphene at the atomic level remains a key challenge in the development of new graphene-based applications. The most common strategy for doing so includes chemical doping,[11-15] functionalisation,[6, 16-22] addition of defects, [23-28] and manipulating the shape/edge structure of the graphene sheets.[29-33] It has been theoretically predicted that creating spatial patterns of functionalised areas including "nanoroads" or 2D quantum dots would lead to novel, hybrid electronic structure in a single graphene sheet,[34, 35] and recently Park et al. succeeded in generating mesoscale patterning, functionalization, and printing on graphene.[36] Nevertheless, the atomic-scale control of functionalization patterning, required for instance in the field of molecular electronics, has not been achieved to date.

The epoxidation of graphene is a notable example of a functionalisation technique that aims to obtain control over flake shape and edge structure.[37-39] Nevertheless, epoxidation, similar to graphene functionalisation in general, also suffers from a lack of regioselective control[21, 40] that in turn limits the utility of such approaches to controlling graphene properties. A number of attempts at regioselective functionalisation of graphene have been reported to date. For instance, a number of groups have reported that graphene epoxidation along specified directions of the graphene lattice can be achieved by straining graphene along the basal plane[37] and at angles perpendicular to the basal plane.[41-43]

Herein we report a strategy for producing curved graphene structures and hence regioselective graphene functionalisation. We show that, by intercalating alkali metal atoms between metal substrates and adsorbed graphene monolayers, the chemical reactivity of the graphene structure becomes highly localised and thus regioselective. This localisation of reactivity is primarily due to the local geometrical deformation of the adsorbed graphene structure, due to the presence of the adsorbed atom. As such, this strategy is most effective for relatively large alkali metals (e.g. potassium), and least effective for smaller metals (e.g. lithium), as in the latter case geometrical distortion in the adsorbed graphene sheet is minimal. We also show that the type of metal substrate employed also influences the extent of this localised reactivity, with nickel substrates leading to more pronounced regioselectivity compared to copper substrates. We propose that this approach, which can exploit existing deposition and lithography techniques[44-46] for controlling the placement of metal atoms on substrates, may potentially enable regioselective functionalisation of graphene structures.

[a] *Newcastle Institute for Energy and Resources, The University of Newcastle, Callaghan 2308 NSW, Australia.*
[b] *Computational Sciences and Engineering Division, Oak Ridge National Laboratory, Oak Ridge, TN 37831, USA*

† Electronic Supplementary Information (ESI) available: Details of carbon atom curvature, charge transfer and charge density difference analyses. See DOI: 10.1039/x0xx00000x

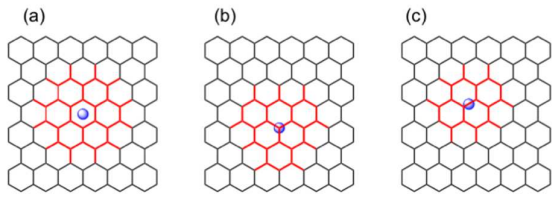

Figure 1. Schematic representation of epoxidation of adsorbed graphene monolayers. The blue sphere represents the position of the alkali metal atom, which is either below a (a) hexagon (b) carbon atom or (c) carbon-carbon bond in the graphene sheet. Red bonds are those which are epoxidated.

Computational Methods

Density Functional Theory Calculations

All DFT calculations were performed using the Vienna Ab Initio Simulation (VASP) Package.[47-50] The Perdew-Burke-Ernzerhof (PBE) exchange correlation functional[51] was used in conjunction with a plane wave energy cut-off of 400 eV and projector augmented-wave (PAW) pseudopotentials.[52] Dispersion was included in all calculations using Grimme's D2 correction.[53] All structures were relaxed fully using convergence criteria of 10^{-3} eV/ Å (forces) and 10^{-4} eV (energy). Brillouin zone sampling was performed using Γ-point sampling, which is sufficient due to the large unit cell dimensions (1.230 nm × 1.278 nm × 5.000 nm). Charge transfer was calculated using the Bader charge analysis method,[54-56] as detailed in the Electronic Supplementary Information (ESI).

Model Interfaces

Model systems consisted of a periodic graphene sheet adsorbed to an underlying metal substrate (1.230 nm × 1.278 nm) with and without an intercalating surface-adsorbed metal atom. The graphene sheet consisted of a rectangular nanoribbon 3 units in the armchair direction and 5 units along the zigzag. Ni and Cu were chosen as the substrates here, since the physical stability and electronic structure of graphene-Ni/Cu interfaces are well understood[57] (due in part to their near-commensurate lattice dimensions) and these substrates are also the most relevant regarding chemical vapour deposition graphene growth (e.g. see ref. [58] and references therein). Graphene-metal interfaces for the (111) and (100) facets consisted of a 5 × 3 graphene monolayer adsorbed onto 5 × 6 × 3 and 5 × 5 × 3 surface slabs, respectively. Three-dimensional periodic boundary conditions were enforced in all calculations. The periodic lattice vectors of all substrate-graphene interfaces were held at those of the graphene sheet. The bottom layer of atoms in the metal substrate was frozen during all geometry optimisations as an approximation to the underlying bulk region. A vacuum region of 5 nm perpendicular to the (111) and (100) surfaces prevented interactions between periodic images normal to the surface.

Li, Na, and K alkali metal atoms were chosen as surface-adsorbed metal atoms since they are an isovalent ns^1 series of highly electropositive elements. This electropositivity enables us to gauge whether or not alkali metal $\rightarrow$ graphene charge transfer is significant in inducing regioselective reactivity in the adsorbed graphene monolayer. Li, Na and K atoms were initially positioned on the model (111) and (100) surfaces consistent with experimentally reported surface structures: on the (100) facets, the alkali metal atoms were placed above the hollow site for both Cu[59-65] and Ni[66, 67]; on the (111) facets, Li and Na were placed above the hollow site, while K was placed directly above a surface atom for both Cu[59, 62, 68, 69] and Ni.[66, 70, 71] For each combination of metal substrate (Ni, Cu) and alkali metal, adsorption of the overlying graphene sheet was modelled with the alkali metal positioned (a) in the middle of a six-membered ring, (b) directly underneath a carbon atom and (c) directly underneath a carbon-carbon bond (Figure 1). In each case, our discussion below only focuses on the most stable configuration obtained from all of these initial starting structures.

Alkali Metal-Induced Regioselectivity in Graphene

Induced regioselective reactivity in graphene is demonstrated here using C-C bond epoxidation. Chemisorption of a single oxygen atom onto the top side of a graphene sheet, relative to the substrate and intercalated alkali metal, serves as a reliable and simple approximation to more complex ligands that bind via comparable mechanisms.[21, 72] Epoxidation is also relevant for controlling the oxidative cutting/etching of graphene sheets.[37, 39, 73, 74] Oxygen atoms were placed directly above carbon-carbon bond midpoints for all bonds in the vicinity of the alkali metal atom. The structure of the entire interface was then fully relaxed. Depending on the position of the alkali metal atom relative to the graphene lattice, the shape and extent of the epoxidated region changed, as shown in Figure 1.

Oxygen chemisorption energy is calculated as,

$$\Delta E = E_{\text{tot}} - E_{\text{O}} - E_{\text{ref}} \quad (1)$$

where E_{ref} is the DFT energy of the reference system (i.e. the substrate-adsorbate-graphene interface, or substrate-graphene interface), E_{O} is the DFT energy of an isolated O atom and E_{tot} is the DFT energy of the epoxidated reference system. At an infinite distance from the alkali metal atom ΔE is expected to converge to the energy of oxidising the substrate-graphene interface (ΔE_{∞}), i.e. in the absence of the alkali metal. ΔE_{∞} can be calculated by applying equation 1 to the reference system without the alkali metal present. We therefore convert all ΔE values into relative chemisorption energies using this reference point,

$$\Delta\Delta E = \Delta E_{\infty} - \Delta E \quad (2)$$

ΔE_{∞} is approximated here as the maximum epoxidation energy in the corresponding substrate-graphene interface without an alkali metal adsorbate. $\Delta\Delta E$ are reported as a function of the distance separating the alkali metal and the respective C-C bond midpoint.

Results and Discussion

Structure of Alkali-Adsorbed Cu and Ni Substrates

The practicality of using surface-adsorbed alkali metal to direct reactivity on physisorbed graphene sheets is limited by the structural integrity of the substrate-adsorbate interface itself.

We therefore begin our discussion by reporting the structure and adsorption energies of the substrate-adsorbate interfaces in the absence of an overlaid graphene sheet, which are summarised in Table 1.

It is immediate from Table 1 that for both (100) and (111) facets of Cu and Ni, the substrate-adsorbate interface is robust. The alkali metal atoms all chemisorb strongly to the Cu(100) substrate; Li binds with an adsorption energy of -271.8 kJ mol^{-1} which is larger than both Na and K, the latter having comparable adsorption energies (-234.2 and -239.6 kJ mol^{-1}, respectively). The distance between the Li, Na and K atoms [Li (1.9 Å) < Na (2.3 Å) < K (2.7 Å)] and the Cu(100) surface is proportional to the alkali metal radii, as anticipated. Comparable trends are observed for the Cu(111) surface, despite some differences in the preferred adsorption sites for these atoms. For instance, while the Cu(111)-adsorbate distances [Li (2.0 Å) < Na (2.4 Å) < K (2.7 Å)] are proportional to the alkali metal radii, Na and Li preferentially adsorb in the surface hollow site consistent with prior experimental results,[59, 62, 68, 69] whereas K preferred to adsorb directly over a surface Cu atom. The latter result is attributed to the larger size of the K atom, which makes it more unfavourable for this atom to intercalate in the Cu(111) surface hollow site. Interestingly however, this makes no difference to K-Cu(111) distance, which is identical to the K-Cu(100) distance despite the different adsorption sites. Further, the trend in the adsorption energies of Li, Na and K observed for Cu(100) is preserved with Cu(111), i.e. Li adsorbs most strongly (-288.9 kJ mol^{-1}), while adsorption of Na and K is weaker (-251.2, -265.0 kJ mol^{-1}, respectively).

The adsorption sites of Li, Na and K on Ni(100) and Ni(111) substrate facets mirror those of their Cu analogues closely, indicating that adsorption site and distance, at least for this series of adsorbates, is primarily determined by the adsorbate size and surface facet, but is independent of the substrate metal. For instance, each atom preferentially adsorbs at a surface hollow site on Ni(100), consistent with experiment,[66, 67] at a comparable distance to that observed for Cu(100) [e.g. Li (1.9 Å) < Na (2.3 Å) < K (2.7 Å)]. Similarly, Li and Na adsorb at a hollow site on Ni(111) at distances of 2.0 and 2.4 Å, respectively, while K adsorbs directly above a Ni atom at 2.7 Å. These results are consistent with prior experiments,[66, 70, 71] and also mirror the results obtained for Cu(111), detailed above. Table 1 shows that the adsorption energies of Li, Na and K on Ni(100) and Ni(111) substrates are consistently ~40 kJ mol^{-1} higher than those on Cu(100) and Cu(111). However, trends in DFT-D2 adsorption energies for the adsorbed alkali metal atoms on Ni(100) and Ni(111) are also consistent with those observed on Cu(100) and Cu(111). For both Ni(100) and Ni(111) substrates, Li adsorbs most strongly, while the DFT-D2 adsorption energies for Na and K are weaker and comparable to each other.

Table 1. DFT-D2 adsorption energies (kJ mol^{-1}) of alkali metal atoms on Cu and Ni (111) and (100) substrate facets. Alkali metal – substrate distance (Å) and adsorption site given in parentheses.

	Cu		Ni	
	(100)	(111)	(100)	(111)
Li	-271.8 (1.9, hollow)	-288.9 (2.0, hollow)	-311.6 (1.9, hollow)	-294.4 (2.0, hollow)
Na	-234.2 (2.3, hollow)	-251.2 (2.4, hollow)	-264.9 (2.3, hollow)	-250.5 (2.4, hollow)
K	-239.6 (2.7, hollow)	-265.0 (2.7, top)	-273.7 (2.7, hollow)	-265.3 (2.8, top)

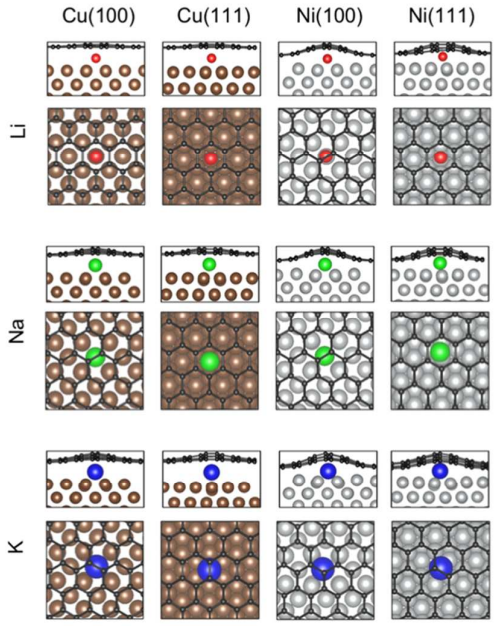

Figure 2. DFT-D2 optimised structures of graphene – adsorbate-metal interfaces for (100) and (111) facets of Cu and Ni substrates, and addsorbed Li, Na and K atoms, shown from above and side. Brown and silver spheres represent Cu and Ni atoms, red, green and blue represent Li, Na and K atoms, and black spheres represent carbon atoms.

Adsorption of Monolayer Graphene on Alkali-Adsorbed Cu and Ni Substrates

We now consider physisorption of monolayer graphene on the alkali metal – adsorbed (100) and (111) substrate facets introduced above. DFT-D2 - optimised structures of each interface are shown in Figure 2. The corresponding adsorption energies of the monolayer graphene sheet on each modified surface facet are provided in Table 2, which also presents adsorption energies of graphene for pristine Cu and Ni (100)/(111) facets for comparison.

The physisorption of monolayer graphene on pristine transition metal substrates has been investigated in a number of previous works.[57, 75] DFT-D2 adsorption energies presented in Table 2 are consistent with these prior results, showing that adsorption of monolayer graphene on Cu is weaker than it is on Ni for both (100) and (111) surface facets. Specifically, Table 2 shows that the adsorption energies on Ni(100) and Ni(111) are ca. twofold those for the Cu(100) and Cu(111) substrates. The introduction of an alkali metal atom to these Cu and Ni substrates generally weakens the physisorption of monolayer graphene.

For instance, on Li-, Na- and K-adsorbed Cu(100) DFT-D2 adsorption energies of monolayer graphene are -7.5, -5.4 and -2.7 kJ mol^{-1} per carbon, respectively. The single exception here is the Li-adsorbed Cu(100) interface, for which the graphene adsorption energy is comparable to that for the

pristine Cu(100) facet itself. The same exception is observed for the modified Cu(111) surfaces; Table 2 shows that the strength of graphene adsorption on pristine and Li-adsorbed Cu(111) are comparable (-8.5 and -8.1 kJ mol^{-1} per carbon, respectively), while that on the Na-adsorbed and K-adsorbed Cu(111) substrate are weaker (-6.0 and -3.3 kJ mol^{-1} per carbon, respectively).

We attribute this trend, i.e. decreasing graphene adsorption energy with increasing atomic radius, to two factors. Firstly, smaller adsorbed atoms allow a larger fraction of the carbon atoms in its vicinity to interact with the substrate, compared to larger adsorbed atoms. Secondly, to adsorb in the presence of the adsorbed atoms the graphene monolayer structure must distort (as shown in Figure 2). Such distortion incurs an energy penalty and makes the adsorption of the graphene sheet weaker overall, and this effect will be proportional to the size of the adsorbed atom. However, the natural affinity of the graphene monolayer for the underlying metal substrate will also be significant in this respect, since the stronger Ni-graphene interactions lead to a more dramatic distortion in the graphene layer around the position of the adsorbed alkali atom.

Figure 3 confirms both of these factors by quantifying the curvature of each carbon atom in the monolayer as a function of distance from the alkali metal atom (curvature is calculated here in the manner of Zheng et al.,[76] see ESI). The distortion of the graphene monolayer near the alkali atom (Figure 2) corresponds to the exponential short-range decrease in the carbon atom curvature (Figure 3). It is immediate from Figure 3 that the largest geometrical distortions (i.e. highest curvatures) to the adsorbed graphene monolayers shown in Figure 2 occur in the presence of the adsorbed K atom, followed by Na and then Li. Figure 3 also shows that the Ni substrates yield greater distortion to the adsorbed graphene structure than do the Cu substrates. This is most notable in the immediate vicinity of the alkali metal atom (e.g. ~within 2-3 Å of the adsorbate), but is also evident in the long range convergence of the carbon atom curvature (e.g. ~5 Å from the adsorbate).

Table 2. DFT-D2 adsorption energies per carbon (kJ mol^{-1}) of monolayer graphene on pristine and alkali metal adsorbed Cu/Ni (100)/(111) substrate facets.

	Cu		Ni	
	(100)	(111)	(100)	(111)
Pristine	-7.4	-8.5	-15.7	-14.1
Li-adsorbed	-7.5	-8.1	-14.3	-12.0
Na-adsorbed	-5.4	-6.0	-11.5	-8.8
K-adsorbed	-2.7	-3.3	-7.4	-4.4

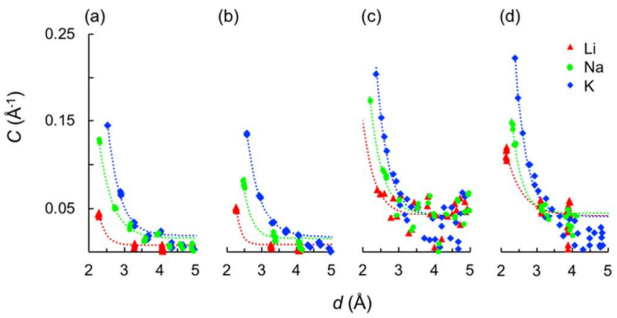

Figure 3. Curvature (C, Å^{-1}) of carbon atoms in graphene – adsorbate-metal interfaces for (a) Cu(100), (b) Cu(111), (c) Ni(100) and (d) Ni(111) substrate facets, as a function of distance (Å) from the adsorbed Li, Na and K atoms. The dotted lines are a visual aid.

Table 3. Maximum ΔΔE values (kJ mol^{-1}) for C-C epoxidation of monolayer graphene on alkali metal adsorbed Cu and Ni substrates (see Figure 4).

	Cu(100)	Cu(111)	Ni(100)	Ni(111)
Li	2.6	21.8	8.6	7.4
Na	27.2	51.1	64.1	33.9
K	37.4	63.6	108.0	115.8

The orientation of the adsorbed alkali metal atom relative to the graphene lattice is a secondary factor regarding the distortion of the graphene monolayer. For instance, Figure 2 shows that the alkali metal atom in the Na-adsorbed Cu(100) substrate is positioned directly under a C-C bond, while for the Cu(111) substrate it is located in the middle of a hexagon. Comparison of Figure 3(a) and (b) shows that the former orientation leads to greater distortion in the graphene structure (i.e. higher curvature). Equivalent trends are observed for the Li and Na adsorbed Ni(100) and Ni(111) substrates, compared in Figure 3(c) and (d).

For all interfaces considered here, the K-adsorbed Cu substrates therefore yield the weakest physisorption of the graphene monolayer. However, adsorption energies for the K-adsorbed Cu(100) and Cu(111) substrates (-2.7 and -3.3 kJ mol^{-1} per carbon atom) correspond to equivalent temperatures of ~325 and 397 K. Monolayer graphene on these substrates will therefore be stable at standard conditions and capable of withstanding further chemical functionalisation. The magnitude of the interaction energy in general will depend on the density of the adsorbed atoms: higher densities will reduce graphene-substrate interaction, compared to the values in Table 2.

Induced Regioselectivity on Distorted Graphene Monolayers

The preceding discussion has established (1) that adsorption of monolayer graphene on modified Cu and Ni substrates is thermodynamically favourable, and (2) that the presence of the alkali metal atom leads to, in some cases, dramatic distortion of the adsorbed graphene structure in the vicinity of the adsorbed atom. It is well known that the reactivity of curved sp^2 hybridized carbon structures is proportional to the local curvature of the network structure.[77] Zheng et al.[76]

established that, in the case of carbon nanotubes, this increased reactivity is primarily due to the perturbation to the π-conjugated electronic structure in the carbon network, and geometrical strain effects. We now demonstrate that the adsorbate-induced curvature of the adsorbed graphene structure yields regioselective reactivity in monolayer graphene structures.

Figure 4 presents ΔΔE of monolayer graphene sheets (Figure 2) adsorbed to alkali metal – adsorbed Cu and Ni substrates. Table 3 summarises the maximum ΔΔE values observed for each modified substrate. ΔΔE is measured relative to a monolayer graphene sheet adsorbed on the respective metal substrate in the absence of the alkali metal atom. Thus, ΔΔE is the indicator of curvature-induced regioselective reactivity in the graphene sheet; C-C bonds for which ΔΔE > 0 have become more reactive due to the presence of the adsorbed alkali metal atom, while those for which ΔΔE < 0 have become less reactive.

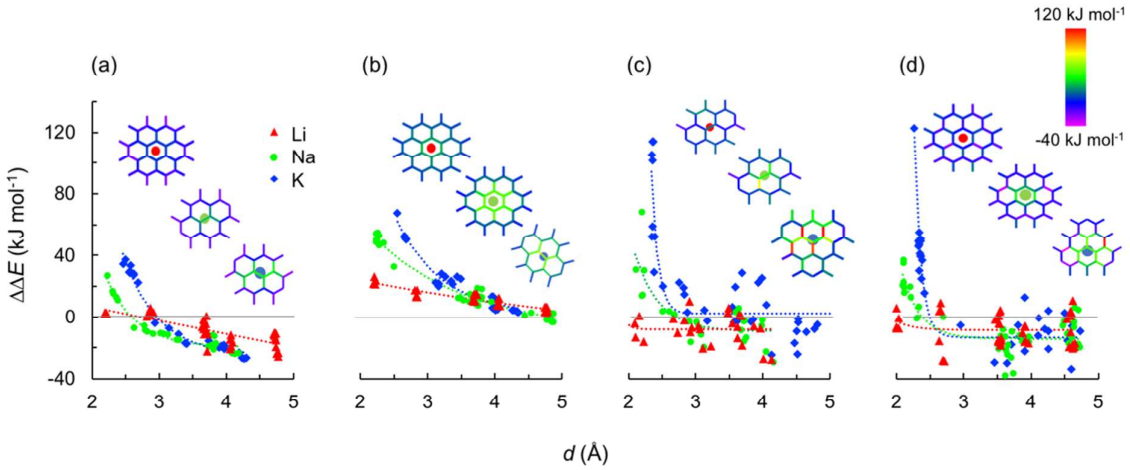

Figure 4. Epoxidation energies ΔΔE (kJ mol^{-1}) of C-C bonds in monolayer graphene adsorbed on alkali metal modified (a) Cu(100), (b) Cu(111), (c) Ni(100) and (d) Ni(111) substrate facets, as a function of distance from the adsorbed Li, Na and K atoms. The dotted lines are a visual aid.

Figure 4 shows that, for all metal substrates considered here, the adsorbed graphene monolayer becomes more reactive in the vicinity of the alkali metal atom. In general, this is most observable for Ni substrates, compared to Cu, a result that is attributed to the stronger graphene-substrate interaction in the case of Ni. The absolute ΔΔE values observed for Cu(100) in Figure 4(a), which are lower than those for the Cu(111) and Ni substrates, are the result of an anomalously stable reference energy, since on Cu(100) the adsorbed graphene monolayer exhibits structural undulations reminiscent of the larger-scale Moiré structure observed in graphene on this substrate.[78]

Trends in ΔΔE observed for each substrate are comparable and independent of the facet (at least for the (100) and (111) facets). The increase in reactivity observed with Li as the adsorbate is minimal, being < 10 kJ mol^{-1} for all substrates considered here. Further, the adsorbed Li induces minimal selectivity, in the sense that there is little, if any, decrease in ΔΔE with increasing distance from the alkali metal atom. Consequently, it is unlikely that Li-adsorbed substrates would afford regioselective reactivity in the graphene monolayer. On the other hand, maximum ΔΔE values for Na and K are significant. In the vicinity of Na and K adsorbates, the adsorbed graphene monolayer is up to ~65 kJ mol^{-1} and ~116 kJ mol^{-1} more reactive, respectively, than a graphene monolayer on a pristine substrate. Na and K adsorbates also yield high selectivity, particularly for Ni(100) and Ni(111) substrates. Figure 4 shows that the decrease in ΔΔE in these cases is exponential with distance. For Na and K adsorbates on Cu, there is a more gradual parabolic decrease in ΔΔE that is nonetheless significant. It is therefore proposed that modifying metal substrates with Na and K may afford a new strategy for controlled, regioselective chemical functionalisation of graphene.

These trends in ΔΔE values are proportional to both the size and electropositivity of the alkali metal atoms, i.e. ΔΔE(K) > ΔΔE(Na) > ΔΔE(Li). The lack of selectivity observed for the Li-adsorbed substrates indicates that adsorbate size (and therefore the extent of induced graphene curvature) is the principle agent of the induced regioselectivity. However, the electropositivity of each alkali metal atom means that electron donation to the unoccupied π* states of the graphene monolayer may partially activate nearby C-C bonds (but not those further away). Indeed, Figures 5 and 6 demonstrate that the adsorbate → graphene charge transfer is highly localised. Figure 6 also confirms that alkali metal electron density is donated to the unoccupied π* states in the graphene structure, but also considerably to the underlying metal substrate d states. Surprisingly however, comparison of Figures 4 and 5 indicate that there is no consistent correlation between this localised charge transfer and the regioselective reactivity in the adsorbed graphene monolayer. We therefore conclude that adsorbate → graphene charge transfer to be a secondary factor, compared to adsorbate-induced geometrical strain of the graphene structure.

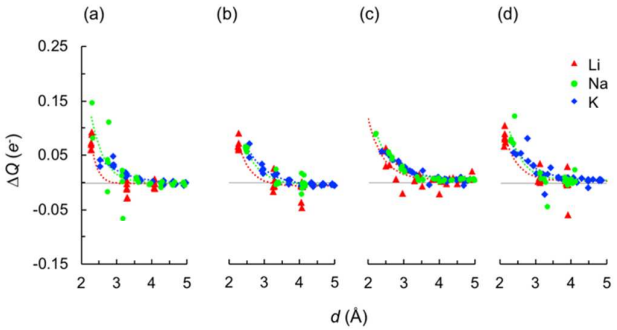

Figure 5. Charge transfer (ΔQ, e^-) for carbon atoms in graphene – adsorbate-metal interfaces for (a) Cu(100), (b) Cu(111), (c) Ni(100) and (d) Ni(111) substrate facets, as a function of distance (Å) from the adsorbed Li, Na and K alkali metal atoms. ΔQ is calculated using Bader charges, relative to a graphene monolayer adsorbed on the corresponding adsorbate-free Cu/Ni facet (see ESI).

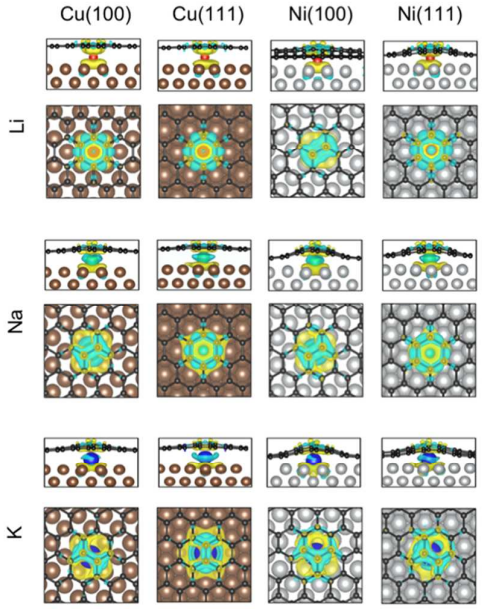

Figure 6. Charge density difference shows charge transfer from Li, Na and K adsorbates to the adsorbed graphene monolayer and underlying metal substrate. Yellow regions of the isosurface indicate increased electron density, and green regions indicate depleted electron density. Atom colours as per Figure 2. Isosurface drawn at 0.001 e/au^3. See ESI for full details of charge density difference analysis.

This suggests that adsorbate-induced regioselective reactivity in graphene is not unique to alkali metals, and can potentially be achieved with arbitrary atomic adsorbates and surface defects (we note that curvature-based reactivity in graphene has been induced using ~50 nm SiO_2 nanoparticles[79]). To demonstrate this possibility, we report $\Delta\Delta E$ for a graphene monolayer adsorbed to an Ar-adsorbed Ni(111) surface in Figure 7(a). In this case, any observed trends in $\Delta\Delta E$ can only be attributed to induced curvature; Ar is an inert noble gas and therefore unlikely to donate charge density to the graphene carbon atoms. Figure 7(a) shows a strong correlation between $\Delta\Delta E$ for the Ar-adsorbed Ni(111) surface and the induced graphene curvature C (Figure 4(b)), despite the atomic radius of Ar (0.71 Å) being smaller than those of Li (1.67 Å), Na (1.90 Å) and K (2.43 Å).[80] Figure 7(c) also shows negligible charge transfer from Ar to the adsorbed graphene monolayer, and hence no correlation between $\Delta\Delta E$ and ΔQ for the surface-adsorbed Ar atom.

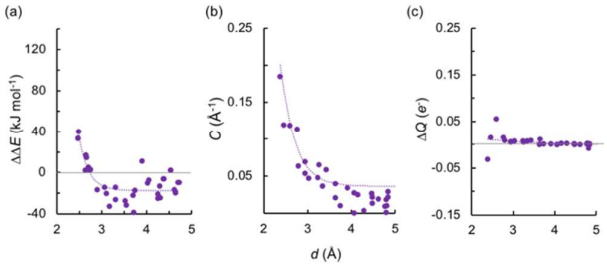

Figure 7. (a) $\Delta\Delta E$ (b) C and (c) ΔQ plots for graphene adsorbed on an Ar-adsorbed Ni(111) substrate. Dotted lines are a visual aid.

Conclusions

In conclusion we have demonstrated that modified metal substrates are capable of inducing localised increases in the chemical reactivity of adsorbed graphene monolayers using first principles calculations. Our results show that on the (100) and (111) facets of Cu and Ni, surface-adsorbed Li, Na and K atoms induce highly localised regions in which epoxidation of an adsorbed graphene monolayer becomes more favourable. The extent of this localised regioselectivity was proportional to both the size of the alkali metal adsorbate atom, and the strength of the graphene-substrate interaction. Notably, regioselective reactivity was limited in the presence of the Li atom, irrespective of the underlying metal substrate. These alkali metal adsorbates are also highly electropositive, however, our analysis of charge transfer between the adsorbates, substrate and graphene monolayer indicates that the electropositivity of the alkali metal atoms is not responsible for the observed regioselective reactivity. This means that the adsorbate-induced geometrical distortion in adsorbed graphene monolayers can be achieved with arbitrary adsorbates and substrate defects, provided such structures are themselves stable, a possibility that has been demonstrated for an Ar-adsorbed Ni(111) substrate. We therefore propose this adsorbate-induced distortion as a potential strategy towards controlling the mesoscale patterning and chemical functionalization of graphene structures.

Acknowledgements

AJP acknowledges support from the Australian Research Council (INTERSECT, LE170100032). IM acknowledges an Australian Postgraduate Award. SI was supported by the Laboratory Directed Research and Development (LDRD) Program of Oak Ridge National Laboratory. ORNL is managed by UT-Battelle, LLC for DOE under Contract DE-AC05-00OR22725. This research was undertaken with the assistance of resources provided at the NCI National Facility systems at the Australian National University and INTERSECT systems, through the National Computational Merit Allocation Scheme supported by the Australian Government. AJP and SI acknowledge vale Prof. Keiji Morokuma (Kyoto University) for enlightening discussions.

Notes and references

1. M. D. Stoller, S. Park, Y. Zhu, J. An and R. S. Ruoff, *Nano Lett.*, 2008, **8**, 3498-3502.
2. A. A. Balandin, S. Ghosh, W. Bao, I. Calizo, D. Teweldebrhan, F. Miao and C. N. Lau, *Nano Lett.*, 2008, **8**, 902-907.
3. C. Lee, X. Wei, J. W. Kysar and J. Hone, *Science*, 2008, **321**, 385-388.
4. K. S. Novoselov, A. K. Geim, S. V. Morozov, D. Jiang, Y. Zhang, S. V. Dubonos, I. V. Grigorieva and A. A. Firsov, *Science*, 2004, **306**, 666-669.
5. E. Pollak, B. Geng, K.-J. Jeon, I. T. Lucas, T. J. Richardson, F. Wang and R. Kostecki, *Nano Lett.*, 2010, **10**, 3386-3388.
6. J. W. Burress, S. Gadipelli, J. Ford, J. M. Simmons, W. Zhou and T. Yildirim, *Angew. Chem., Int. Ed.*, 2010, **49**, 8902-8904.
7. Q. Ji, I. Honma, S.-M. Paek, M. Akada, J. P. Hill, A. Vinu and K. Ariga, *Angew. Chem., Int. Ed.*, 2010, **49**, 9737-9739.
8. F. Schedin, A. K. Geim, S. V. Morozov, E. W. Hill, P. Blake, M. I. Katsnelson and K. S. Novoselov, *Nature Mater.*, 2007, **6**, 652.
9. Y. Si and E. T. Samulski, *Nano Lett.*, 2008, **8**, 1679-1682.
10. V. Georgakilas, M. Otyepka, A. B. Bourlinos, V. Chandra, N. Kim, K. C. Kemp, P. Hobza, R. Zboril and K. S. Kim, *Chem. Rev.*, 2012, **112**, 6156-6214.
11. S. Agnoli and M. Favaro, *J. Mater. Chem. A*, 2016, **4**, 5002-5025.
12. R. Yadav and C. K. Dixit, *J. Sci.: Adv. Mater. Dev.*, 2017, **2**, 141-149.
13. M. An, C. Du, L. Du, Y. Sun, Y. Wang, C. Chen, G. Han, G. Yin and Y. Gao, *Chem. Phys. Lett.*, 2017, **687**, 1-8.
14. Z. Wang, P. Li, Y. Chen, J. Liu, W. Zhang, Z. Guo, M. Dong and Y. Li, *J. Mater. Chem. C*, 2015, **3**, 6301-6306.
15. H. Mousavi, *Phys. B*, 2013, **414**, 78-82.
16. A. L. Higginbotham, D. V. Kosynkin, A. Sinitskii, Z. Sun and J. M. Tour, *ACS Nano*, 2010, **4**, 2059-2069.
17. A. J. Page, C.-P. Chou, B. Q. Pham, H. A. Witek, S. Irle and K. Morokuma, *Phys. Chem. Chem. Phys.*, 2013, **15**, 3725-3735.
18. S. Uruş, M. Çaylar and İ. Karteri, *Chem. Eng. J.*, 2016, **306**, 961-972.
19. S. M. Avdoshenko, I. N. Ioffe, G. Cuniberti, L. Dunsch and A. A. Popov, *ACS Nano*, 2011, **5**, 9939-9949.
20. T. Takahashi, K. Sugawara, E. Noguchi, T. Sato and T. Takahashi, *Carbon*, 2014, **73**, 141-145.
21. J. Park and M. Yan, *Acc. Chem. Res.*, 2013, **46**, 181-189.
22. J. E. Johns and M. C. Hersam, *Acc. Chem. Res.*, 2013, **46**, 77-86.
23. L. Vicarelli, S. J. Heerema, C. Dekker and H. W. Zandbergen, *ACS Nano*, 2015, **9**, 3428-3435.
24. S. Singha Roy, R. M. Jacobberger, C. Wan and M. S. Arnold, *Carbon*, 2016, **100**, 1-6.
25. Q. Xu and W. Zhang, in *Advances in Carbon Nanostructures*, eds. A. M. T. Silva and S. A. C. Carabineiro, InTech, Rijeka, 2016, p. Ch. 02.
26. B. Yang, S. Wang, Y. Guo, J. Yuan, Y. Si, S. Zhang and H. Chen, *RSC Adv.*, 2014, **4**, 54677-54683.
27. H. Chen and E. Ruckenstein, *J. Phys. Chem. Lett.*, 2014, **5**, 2979-2982.
28. S. Wang, B. Yang, H. Chen and E. Ruckenstein, *J. Mater. Chem. A*, 2018, **6**, 6815-6821.
29. M. Terrones, A. R. Botello-Méndez, J. Campos-Delgado, F. López-Urías, Y. I. Vega-Cantú, F. J. Rodríguez-Macías, A. L. Elías, E. Muñoz-Sandoval, A. G. Cano-Márquez, J.-C. Charlier and H. Terrones, *Nano Today*, 2010, **5**, 351-372.
30. T. S. Li, M. F. Lin, C. Y. Lin, S. C. Chang and S. P. Yang, *Synth. Met.*, 2013, **171**, 7-14.
31. K. Nakada, M. Fujita, G. Dresselhaus and M. S. Dresselhaus, *Phys. Rev. B*, 1996, **54**, 17954-17961.
32. Z. Chen, Y.-M. Lin, M. J. Rooks and P. Avouris, *Phys. E*, 2007, **40**, 228-232.
33. F. Ma, Z. Guo, K. Xu and P. K. Chu, *Solid State Commun.*, 2012, **152**, 1089-1093.
34. A. K. Singh, E. S. Penev and B. I. Yakobson, *ACS Nano*, 2010, **4**, 3510-3514.
35. M. A. Ribas, A. K. Singh, P. B. Sorokin and B. I. Yakobson, *Nano Res.*, 2011, **4**, 143-152.
36. J. Park, H.-K. Park and J. Choi, *J. Phys. Chem. C*, 2017, **121**, 14954-14961.
37. L. Ma, J. Wang and F. Ding, *Angew. Chem., Int. Ed.*, 2012, **51**, 1161-1164.
38. J.-L. Li, K. N. Kudin, M. J. McAllister, R. K. Prud'homme, I. A. Aksay and R. Car, *Phys. Rev. Lett.*, 2006, **96**, 176101.
39. T. Sun and S. Fabris, *Nano Lett.*, 2012, **12**, 17-21.
40. X. Wang and G. Shi, *Phys. Chem. Chem. Phys.*, 2015, **17**, 28484-28504.
41. X. Gao, Y. Wang, X. Liu, T. L. Chan, S. Irle, Y. Zhao and S. B. Zhang, *Phys. Chem. Chem. Phys.*, 2011, **13**, 19449-19453.
42. Z. F. Wang, Y. Zhang and F. Liu, *Phys. Rev. B*, 2011, **83**, 041403.
43. L. A. Chernozatonskii and P. B. Sorokin, *J. Phys. Chem. C*, 2010, **114**, 3225-3229.
44. S. R. Schofield, N. J. Curson, M. Y. Simmons, F. J. Rueß, T. Hallam, L. Oberbeck and R. G. Clark, *Phys. Rev. Lett.*, 2003, **91**, 136104.
45. D. P. Adams, T. M. Mayer and B. S. Swartzentruber, *Appl. Phys. Lett.*, 1996, **68**, 2210-2212.
46. S. W. Schmucker, N. Kumar, J. R. Abelson, S. R. Daly, G. S. Girolami, M. R. Bischof, D. L. Jaeger, R. F. Reidy, B. P. Gorman, J. Alexander, J. B. Ballard, J. N. Randall and J. W. Lyding, *Nature. Comm.*, 2012, **3**, 935.
47. G. Kresse and J. Hafner, *Phys. Rev. B*, 1993, **47**, 558-561.

48. G. Kresse and J. Hafner, *Phys. Rev. B*, 1994, **49**, 14251-14269.
49. G. Kresse and J. Furthmüller, *Comp. Mater. Sci.*, 1996, **6**, 15-50.
50. G. Kresse and J. Furthmüller, *Phys. Rev. B*, 1996, **54**, 11169-11186.
51. J. P. Perdew, K. Burke and M. Ernzerhof, *Phys. Rev. Lett.*, 1996, **77**, 3865-3868.
52. G. Kresse and D. Joubert, *Phys. Rev. B*, 1999, **59**, 1758-1775.
53. S. Grimme, *J. Comput. Chem.*, 2006, **27**, 1787-1799.
54. R. F. W. Bader, *Atoms in Molecules: A Quantum Theory*, Clarendon Press, 1994.
55. E. Sanville, S. D. Kenny, R. Smith and G. Henkelman, *J. Comput. Chem.*, 2007, **28**, 899-908.
56. W. Tang, E. Sanville and G. Henkelman, *J. Phys.: Condens. Matter*, 2009, **21**, 084204.
57. G. Giovannetti, P. A. Khomyakov, G. Brocks, V. M. Karpan, J. van den Brink and P. J. Kelly, *Phys. Rev. Lett.*, 2008, **101**, 026803.
58. B. McLean, C. A. Eveleens, I. Mitchell, G. B. Webber and A. J. Page, *Phys. Chem. Chem. Phys.*, 2017, **19**, 26466-26494.
59. G. G. Rusina, S. V. Eremeev, P. M. Echenique, G. Benedek, S. D. Borisova and E. V. Chulkov, *J. Phys.: Condens. Matter*, 2008, **20**, 224007.
60. P. Rudolf, C. Astaldi, G. Cautero and S. Modesti, *Surf. Sci.*, 1991, **251-252**, 127-131.
61. J. Ellis and J. P. Toennies, *Phys. Rev. Lett.*, 1993, **70**, 2118-2121.
62. C. Astaldi, P. Rudolf and S. Modesti, *Solid State Commun.*, 1990, **75**, 847-850.
63. A. P. Graham and J. P. Toennies, *Phys. Rev. B*, 1997, **56**, 15378-15390.
64. A. P. Graham, J. P. Toennies and G. Benedek, *Surf. Sci.*, 2004, **556**, L143-L149.
65. P. Senet, J. P. Toennies and G. Witte, *Chem. Phys. Lett.*, 1999, **299**, 389-394.
66. R. L. Gerlach and T. N. Rhodin, *Surf. Sci.*, 1969, **17**, 32-68.
67. U. Muschiol, P. Bayer, K. Heinz, W. Oed and J. B. Pendry, *Surf. Sci.*, 1992, **275**, 185-189.
68. S. Å. Lindgren, C. Svensson, L. Walldén, A. Carlsson and E. Wahlström, *Phys. Rev. B*, 1996, **54**, 10912-10916.
69. S. Å. Lindgren, C. Svensson and L. Walldén, *J. Electron. Spectrosc. Relat. Phenom.*, 1993, **64**, 483-490.
70. D. Fisher, S. Chandavarkar, I. R. Collins, R. D. Diehl, P. Kaukasoina and M. Lindroos, *Phys. Rev. Lett.*, 1992, **68**, 2786-2789.
71. S. Chandavarkar, R. D. Diehl, A. Faké and J. Jupille, *Surface Science*, 1989, **211-212**, 432-440.
72. K. P. Loh, Q. Bao, P. K. Ang and J. Yang, *J. Mater. Chem.*, 2010, **20**, 2277-2289.
73. J. Pengfei, P. Fengming and C. Tianhang, *IOP Conference Series: Materials Science and Engineering*, 2017, **182**, 012030.
74. H. Al-Mumen, F. Rao, W. Li and L. Dong, *Nano-Micro Lett.*, 2014, **6**, 116-124.
75. A. J. Page, Y. Wang, H.-B. Li, S. Irle and K. Morokuma, *J. Phys. Chem. C*, 2013, **117**, 14858-14864.
76. G. Zheng, Z. Wang, S. Irle and K. Morokuma, *J. Am. Chem. Soc.*, 2006, **128**, 15117-15126.
77. Z. Chen, W. Thiel and A. Hirsch, *ChemPhysChem*, 2003, **4**, 93-97.
78. J. Cho, L. Gao, J. Tian, H. Cao, W. Wu, Q. Yu, E. N. Yitamben, B. Fisher, J. R. Guest, Y. P. Chen and N. P. Guisinger, *ACS Nano*, 2011, **5**, 3607-3613.
79. Q. Z. Wu, Y. P. Wu, Y. F. Hao, J. X. Geng, M. Charlton, S. S. Chen, Y. J. Ren, H. X. Ji, H. F. Li, D. W. Boukhvalov, R. D. Piner, C. W. Bielawski and R. S. Ruoff, *Chem. Commun.*, 2013, **49**, 677-679.
80. E. Clementi, D. L. Raimondi and W. P. Reinhardt, *J. Chem. Phys.*, 1967, **47**, 1300-+.

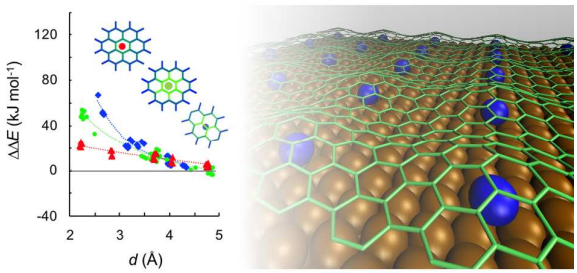

Intercalating alkali metal atoms between metal substrates and adsorbed graphene monolayers yields curvature-induced regioselective reactivity of graphene